Nuclear Materials and Energy 30 (2022) 101137

Contents lists available at ScienceDirect

Nuclear Materials and Energy

journal homepage: www.elsevier.com/locate/nme

Influence of thin surface oxide films on hydrogen isotope release from ion-irradiated tungsten

K. Kremer [a,b], M. Brucker [a,1], W. Jacob [a], T. Schwarz-Selinger [a]

[a] Max Planck Institute for Plasma Physics, 85748 Garching, Germany
[b] Physik-Department E28, Technische Universität München, 85748 Garching, Germany

ARTICLE INFO

Keywords:
Hydrogen Isotope retention
Tungsten oxide
TDS
NRA
Hydrogen isotope release
Deuterium release
Thin films
D release from tungsten
Water formation

ABSTRACT

We studied the influence of thin, electro-chemically grown tungsten (W) surface oxide films on hydrogen isotope release from W. As deuterium (D) reservoir underneath the oxide, we used a defect-rich, ion-irradiated W layer that was filled with D prior to oxidation. Several oxide films with thicknesses between 5 and 100 nm were studied and compared with tungsten with a natural oxide film. The release of D through the oxide film was analyzed with thermal desorption spectroscopy (TDS). The depth-resolved concentration profiles of D in the sample were measured with nuclear reaction analysis at all experimental steps. Changes of the morphology of the oxide film due to the release of D were investigated with scanning electron microscopy (SEM).

In TDS studies, we found that the thin oxide films significantly influence the release behavior of D from W. The first D release peak (at 560 K) is shifted towards higher temperature (or later times) with increasing oxide thickness. This indicates that the oxide film acts as both a D reservoir and a transport barrier that delays D release at temperatures above 475 K. At this temperature, D also starts to interact chemically with the oxide film and is released not only as HD or D_2 but also in the form of heavy water (HDO and D_2O). Above 700 K, D is released only in form of heavy water as long as enough oxide is available. Accordingly, SEM images after TDS show a strong modification of the oxide film. For film thicknesses of 5–10 nm, all oxide is removed from the surface and smooth metallic W remains. For 15 nm, the surface is still partially covered by oxide islands with several micrometer of metallic W between them. From the fact that D is still only released as heavy water at high temperatures, we conclude that the mobility of D atoms at the surface is very high. Even D atoms that surface far from an oxide island apparently travel along the surface to form an O-D group at the W oxide before they recombine with another D atom to form water.

Our results indicate that the oxide film becomes relevant for the D release during TDS if the ratio of O atoms on the surface to D atoms in the sample is larger than 5–10 %. Consequently, even the natural oxide film (1–2 nm) that forms on W upon contact with air may significantly influence the D release spectra from TDS for experiments with low D retention.

1. Introduction:

Tungsten (W) is the material of choice for the divertor of the future experimental fusion reactor ITER [1] and a candidate material for divertor and main wall armor of the planned demonstration fusion reactor DEMO [2]. The main advantages of W are its high threshold for physical sputtering, high melting point and low intrinsic hydrogen isotope (HI) retention [3]. The low retention of HIs and especially of the radioactive tritium fuel is vital for fusion reactors to keep the tritium inventory of the reactor wall low and to conserve the valuable tritium fuel. However, HI uptake, retention and release from W under reactor conditions is still subject to discussion [4], as the fusion plasma imposes several degrading effects on the wall material. Especially the bombardment with 14.1 MeV neutrons from the D, T fusion reaction creates additional defects in the wall material that can bind HIs [5]. These defects or HI "traps" can increase the total HI retention in W by several orders of magnitude compared with un-irradiated W [6]. In recent years, several laboratory experiments on HI release from W [7–11] have been conducted in order to gain a fundamental understanding of the role that irradiation defects in W play in HI retention and release. As no neutron source in this energy range is available, these experiments used high-energy ions as a substitute to create displacement

[1] Present address: Max Planck Institute for Solid State Research, Heisenbergstrasse 1, D-70569 Stuttgart, Germany.

https://doi.org/10.1016/j.nme.2022.101137
Received 23 December 2021; Received in revised form 27 January 2022; Accepted 12 February 2022
Available online 16 February 2022

damage. Often MeV-energy tungsten ions are used as such self-ion implantation avoids inserting foreign elements into the material that may influence retention due to additional chemical effects [12]. Deuterium (D) is commonly used as substitute for tritium. The D release is then commonly investigated with thermal desorption spectroscopy (TDS) where the release behavior of HIs is monitored over a temperature interval up to 1000 K or higher. With known trap- and D concentration profiles, retention and release can be modeled by macroscopic rate equation codes such as TMAP, MHIMES or TESSIM-X [13–15]. By repeating such experiments for different exposure conditions or with different temperature ramps or holding temperatures, the binding energies of HIs in traps in W can be derived [7,9,14,16,17]. Thus, the results of these well-defined, laboratory experiments have established a solid foundation for understanding HI retention and release from (irradiation-) damaged W.

However, recent studies by Hodille et al. [8] have indicated that also thin surface oxides on the W samples may have an influence on the D retention and release in W. As W has an affinity for oxygen, such natural surface oxide films with thicknesses of 1–2 nm are always present on W in *ex situ* laboratory studies (and also in *in situ* studies, if not great care is taken to remove them) [8,18]. However, they may not be present in the divertor or first wall of a fusion reactor, where they could be quickly eroded by the fusion plasma [19]. In this case, effects the natural oxide films might have would represent an unaccounted difference between laboratory studies and reactor relevant conditions that needs to be understood to make correct prediction from laboratory experiments to reactor conditions. On the other hand, the oxidation state of the W armor of a fusion reactor first wall or divertor may be very different depending on the location. It might also be that oxide films that are even thicker than the natural oxide may form in low-flux areas under the given vacuum conditions. In that second case, the here-studied thicker oxide films may even be directly relevant for a fusion reactor scenario. Clearly, a detailed understanding of the effects that natural oxide films have on the retention and release of HIs with W is necessary to interpret the results of laboratory experiments correctly and to enable the extrapolation of these results to reactor-relevant conditions.

Experiments to clarify the influence of oxide films on D release are hampered by several issues. First, D retention in tungsten is typically lower than in tungsten oxide [20]. Consequently, D desorption during TDS would be dominated by the D retained in the oxide itself rather than by the D retained in the underlying bulk W. Second, thermal oxidation of deuterium-containing tungsten is also not a viable option, as most of the retained deuterium would be released at the necessary oxidizing temperatures. Thirdly, thick oxide films (μm scale) are known to crack due to their volume difference to W and data interpretation is then ambiguous [20].

In a recent publication, the influence of thin oxide films on D uptake in tungsten was studied [21]. Complementary to that, the aim of this present study is to clarify which - if any - effect thin oxide films have on D release from tungsten. In order to achieve this, a novel approach has been devised in which a MeV-W-ion-irradiated layer of W was used as a D reservoir underneath an oxide film. After loading this W layer with D in a gentle plasma, the samples were electro-chemically oxidized to oxide film thicknesses of 5 to 100 nm. Release spectra of D molecules and D-containing molecules were monitored during thermal desorption experiments.

This article is structured in the following way. First, the novel methodology is outlined. Second, sample preparation and the analysis methods are presented. After that, the results are discussed in detail and the implications for HI release experiments from W are discussed. Lastly, the results and implications are summarized and a conclusion of the role of oxide films for D release from laboratory experiments is drawn.

2. Methodology:

The goals of this study are to:

a) clarify how thin surface oxide films affect the release of HIs from ion-irradiated W,
b) investigate the transport of HIs through the oxide film and to study to what extend outgassing HIs interact with the oxide film and
c) extrapolate towards the effects that thin (1–2 nm), natural oxide films may have on TDS results in general.

In order to achieve these goals a novel approach has been employed: A W-ion-irradiated layer of W was used as a HI reservoir underneath the oxide film. The experimental approach is illustrated in Fig. 1. As a first step, we induce a 2.3 μm thick, defect-rich layer of so-called "self-damaged" W (dark grey) by bombarding a well-annealed polycrystalline W sample with 20.3 MeV W^{6+} -ions. This self-damaged region incorporates a high concentration of material defects that locally enhances D retention [22]. Next, the material defects in this self-damaged region are decorated with low-energy D (<5 eV/D) from a plasma. The total D amount as well as the D concentration profile are then characterized with ^{3}He nuclear reaction analysis (NRA). Thus, we have an absolutely quantified D reservoir. After that, the sample is electro-chemically oxidized to oxide thicknesses of 5 to 100 nm. This oxidation method was originally designed for gradual removal of W [23] and works at room temperature, i.e., it does not cause the thermal release of D trapped in the self-damaged layer. The produced oxide films are characterized by Rutherford backscattering spectrometry (RBS) and NRA. In a final step, the D outgassing from the self-damaged W through the oxide film is measured with thermal desorption spectroscopy (TDS). Finally, NRA is applied after the thermal treatment to quantify any possibly remaining D and the change in the oxide amount. Additionally, changes in the oxide films are monitored with scanning electron microscopy (SEM) of the surfaces of the oxide film and of cross sections through the oxide film.

In a first batch of experiments, oxide thicknesses of 25, 50 and 100 nm were chosen because they were expected to be thick enough to yield a measurable effect, but still thin enough not to develop macroscopic cracks during growth. Later on, also a second batch of thinner oxides (5, 10 and 15 nm) was examined to approach the thickness of the natural oxide (1–2 nm) more closely.

3. Sample preparation and analysis methods:

3.1. Sample preparation

All samples used in this study, are cut from a single sheet of hot-rolled W with a purity of 99.97 wt.% supplied by Plansee [24]. They

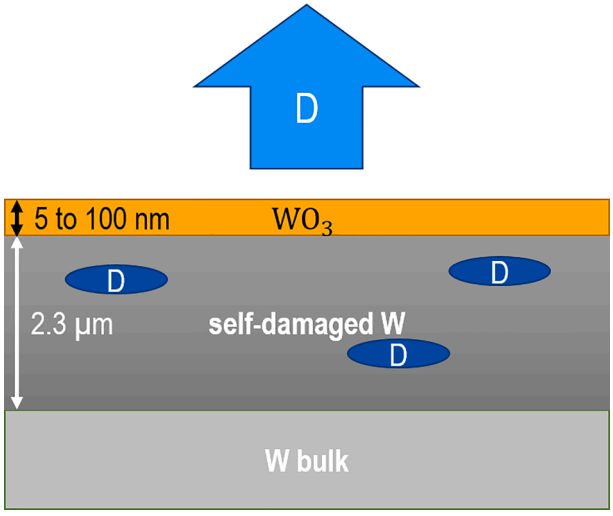

Fig. 1. Schematic of self-damaged, deuterium-decorated and electro-chemically oxidized W sample. The self-damaged zone (dark grey) serves as a quantified D reservoir during TDS.

are $15 \times 11.8 \times 0.8$ mm^3 in size and are individually numbered by laser engraving on the backside.

First, the sample surface is mechanically grinded and then electro-polished in 1.5 % NaOH to achieve a mirror-like finish [25]. The samples are then cleaned in an ultrasonic bath in two steps, first with acetone then with isopropanol for 20 min each before being rinsed in distilled water.

Next, the samples are annealed by electron-beam heating in ultra-high vacuum (base pressure $< 5 \times 10^{-7}$ Pa, rising to $< 3 \times 10^{-5}$ Pa during annealing) at 2000 K for 5 min. This reduces the defect density in the bulk and thus minimizes its contribution to the total HI retention in the sample. Additionally, the heating allows grain growth to a diameter of $\approx$10–50 μm [21], which minimizes the possible effects of grain boundaries on HI transport and retention.

3.2. Self-ion-damaging

After annealing, the samples are irradiated with 20.3 MeV W^{6+} ions at 300 K at the TOF beamline of the tandem accelerator laboratory. The ion beam is scanned across the sample surface to achieve a laterally homogenous irradiation with a fluence of 7.87×10^{13} W/cm^2 [22]. This creates a self-damaged zone in the first 2.3 μm of the W sample with a maximum calculated displacement damage of 0.23 displacements per atom (dpa) [22]. During implantation, a molybdenum mask with an opening of 10×14 mm^2 is used to hold the samples in place. It shields the edges of the sample from the W-ion bombardment and leaves an un-damaged rim along the sample edges.

The self-damaging is essential for the experiments as it introduces a well-controlled amount of defects in the material without changing the elemental composition. These defects later act as traps for HIs, which enhance the HI retention in the self-damaged region by more than two orders of magnitude [6] compared with the underlying bulk W, so that the total HI retention in the sample is now governed by the self-damaged zone. It is important to note that de-trapping energies for HIs that are bound in these traps range between 1.18 and 1.84 eV [9]. As a consequence, the samples show no D release over time as regularly observed for un-damaged tungsten [10,26].

3.3. Deuterium plasma-loading of self-damaged layer

After the self-damaging, the samples were exposed to a gentle D plasma in the low-temperature plasma device "PlaQ". A detailed description of the setup is given in Refs. [27,28]. In the experiments reported here, the sample temperature is kept at 370 K during plasma exposure, which is high enough to allow for D mobility and low enough to avoid significant annealing of the displacement damage that was introduced during the self-damaging. The sample holder has a feedback-controlled temperature regulation so that the exposure temperature is independent from the ion flux.

To assure a homogeneous D filling level across the samples, the existing defects in the self-damaged layer have to be saturated with D. In addition, the loading has to be "gentle" enough to avoid the creation of new defects during plasma exposure that would lead to dynamic release during storage (see [10,26]). Therefore, the samples were exposed to a high D fluence at a low D flux at a D ion energy of < 5 eV/D and substrate temperature of 370 K. These parameters avoid the creation of additional defects during plasma loading as studied in detail in [29]. The average ionic D flux to the sample is 5.6×10^{15} D/(cm^{2}s), and drops with radial distance from the center position of the sample holder by $<$10 % over the samples surface.

The samples were exposed in two different batches (a third batch was not exposed and serves as reference for purely thermally introduced changes in the oxide during TDS; see section 4.1). The first batch contained the samples that were later oxidized to thicknesses of 25, 50 and 100 nm and a reference sample that has only natural oxide (1–2 nm), but was also self-damaged prior to D loading. Whereas the second batch contained samples that were later oxidized to 5, 10 and 15 nm. The first batch was exposed to the plasma for 72 h accumulating a total fluence of 1.5×10^{21} D/cm^2. After the exposure when the D content was measured with NRA, it became clear that the samples from the first batch exhibit a gradient of 10 % in the D content from sample top to bottom, i.e., in radial direction on the sample holder. This indicates that these samples were not filled with D up to the maximum possible retention everywhere on the sample surface. For the second batch, the exposure time was increased to 96 h and a total D fluence of 2.0×10^{21} D/cm^2. These samples exhibited a uniform D content across the sample with a total D retention of 2.3×10^{17} D/cm^2 in the self-damaged layer. In the following all measurements concerning the D content or change thereof in the first batch have been normalized with the D content at each given measurement position, so that the D gradient is accounted for and does not further influence any statements or conclusions drawn in this article.

3.4. Electro-chemical, low-temperature oxidation

After the D "reservoir" was filled, the samples were electro-chemically oxidized to film thicknesses of 5, 10, 15, 25, 50 and 100 nm, respectively. The electro-chemical oxidation method we used was originally devised by McCargo et al. [23] for precise removal of thin films of tungsten via oxidation and subsequent oxide dissolution in NaOH. To our best knowledge, it is used for the first time to deliberately create W oxide films to study D release from W. For oxidation, the W sample was used as anode and immersed in an aqueous solution of 0.4 mol/l KNO_3 and 0.04 mol/l HNO_3. Two W sheets were also immersed and used as cathodes. The voltage for the desired oxide thickness (see [23]) was then applied with a constant current limitation of 2 mA/cm^2 with regard to the sample (and W holding clamp) surface area. The voltage drop across the oxide then grows with the oxide thickness. After reaching the maximum voltage, the voltage was kept constant for one minute (during which the sample current decreased further). After that, the voltage was switched-off and the sample was removed and rinsed in distilled water before immediately drying it.

The main benefit of this method, as compared with thermal oxidation, is that it works at room temperature. This makes it possible to oxidize the surface of the tungsten sample without causing a thermal release of the trapped D in the self-damaged zone. Furthermore, the method works on a timescale of minutes rather than of hours or days as it would be the case for thermal oxidation (compare with our previous work [21]). Another advantage of these films is their smoothness as can be seen in Fig. 2 where SEM images of one electro-chemically grown oxide and one thermally grown oxide are shown for comparison. While the electro-chemically grown oxide film (Fig. 2a) is very smooth inside the individual grains, the thermally grown oxide (Fig. 2b) shows a nano-crystalline microstructure. A further advantage is that the oxide thickness does not depend on the orientation of the underlying W grain as is the case for thermally grown oxide films [30]. This is because the oxide film thickness is determined by the applied voltage and not by different growth rates on different crystal orientations. It should, however, be noted that, as observed by Raman and Infrared spectroscopy [31,32], the electro-chemically grown W oxide has an amorphous structure and thus may differ from thermally grown, nano-crystalline W oxide or from the natural oxide that grows at room temperature on W. A more detailed characterization of the electrochemically grown oxides with these techniques is presently under way and will be the content of an upcoming publication.

3.5. Thermal desorption spectroscopy

Thermal desorption spectroscopy (TDS) is an analysis method allowing to study the release behavior of gaseous inclusions from solids. It can potentially provide information about binding energies, the number of desorbed particles and possibly their desorption mechanisms. In this work, D is trapped in material defects in the self-damaged W layer

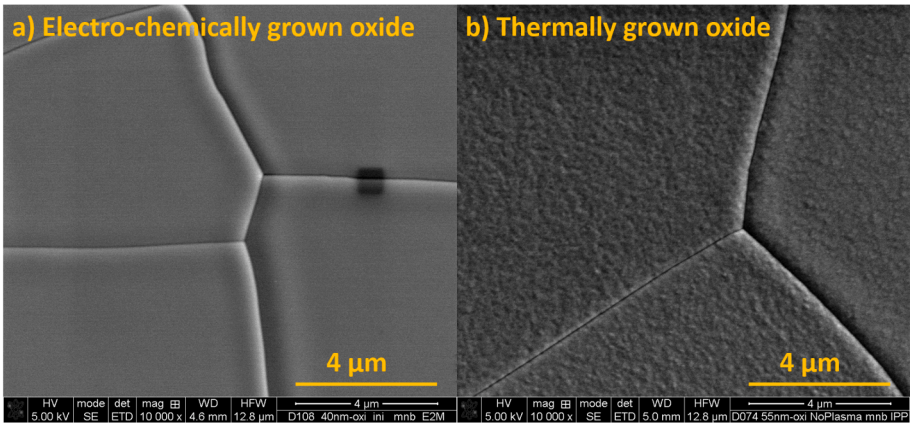

Fig. 2. Secondary electron SEM images of W surface oxides. a) electro-chemical grown oxide (40 nm) b) thermally grown oxide (55 nm) prepared at 600 K at atmospheric pressure in a dry mixture of 80 % argon and 20 % oxygen.

underneath the oxide film. The D will be released from the defects once the sample temperature is sufficiently high for thermal de-trapping. In previous experiments without an artificial oxide film on the W, a double peak structure of the D release was observed [9]. An example for such a TDS spectrum will be later discussed in Fig. 8 for the un-oxidized, self-damaged W reference sample. Details on the determination of binding energies of D traps in W from TDS spectra can be found elsewhere [14,16,17]. In this work, the focus lies on how the oxide film affects the release behavior, i.e., if the D release peak temperature and the composition of released D-containing species are altered.

The TDS setup used in this work is the ultra-high vacuum (UHV) device TESS (Thermal Effusion Spectroscopy Setup). A detailed description of the setup is given in [33,34]. The samples are loaded into a quartz tube that is connected to the main UHV chamber. Samples inside the tube can be heated by an external tube furnace (single wire wound Gero SR 40–250/11), which can be moved over the quartz tube. Several samples can be stored in a side arm of the quartz tube far away from the heating area and can be moved to the heating area via a piece of nickel that is manipulated by an external magnet. Thus, batches of several samples can be measured under identical vacuum conditions. Furthermore, this setup has two advantages: a) it allows outgassing of the quartz tube prior to the sample measurement and b) it does not need a sample holder, which could contaminate the measurement by outgassing. The oven temperature is programmed and feedback controlled so that it undergoes a linear temperature ramp. The actual sample temperature is lower than the oven temperature and lags behind it depending on the ramping speed and the emissivity of the sample surface. Therefore, the temperature in the quartz tube is measured separately via a shielded thermo-couple touching the sample surface. The TDS measurements in this work were all performed with a slow temperature ramp of 3 K/min from room temperature up to 1000 K. This slow ramp together with the inside thermocouple assures an excellent reproducibility of the sample temperature. Near the onset of the temperature ramp ($T < 500$ K), the reproducibility in the sample temperature measurement is better than 10 K. For temperatures above 600 K, which are most relevant for D release, the variation is even smaller and lies well below 5 K. In all TDS spectra in this work, the temperature reading of this shielded thermocouple and not the oven temperature is shown.

The desorbed gases were measured with a Pfeiffer/Inficon DMM 422 quadrupole mass spectrometer (QMS) whose detector was operated in single-ion-counting mode. This allows applying Poisson statistics and assures negligible background noise. The following 15 mass channels were recorded with the so-called multiple ion detection mode: $m/z = 1$, 2, 3, 4, 12, 14, 16, 17, 18, 19, 20, 28, 32, 40 and 44. Residual backgrounds were measured before as well as after the temperature ramp as well as during ramps without a sample in the hot zone. Background subtraction and absolute calibration was conducted for mass channels 3, 4, 19 and 20 to derive absolute fluxes of D_2, HD, HDO and D_2O. The calibration procedure for HD and D_2 follows the description in [9]. The calibration of heavy water species will be discussed in detail in a separate upcoming publication [35] as a full description is beyond of the scope of this work. Here we want to introduce only a short outline of the principle: The calibration utilizes the fact that the absolute amount of D in the oxidized samples was in addition measured with NRA before and after TDS (see section 4.2). Thus, the absolute amount of D released in total (from NRA) and the absolute amount of D released in form of HD and D_2 (from TDS) can be determined. By closing the D balance, the absolute amount of D released in form of HDO and D_2O can be obtained and related to the measured counts in mass channels 19 and 20.

The TDS measurements were performed in two different measurement campaigns for the three batches of samples that are discussed in Section 3.3. The reference sample was exposed in batch one.

3.6. Oxide characterization

The oxygen areal density of the oxide film was determined *ex situ* by RBS with ^{3}He ions (energy range 1.2 to 2.4 MeV, perpendicular angle of incidence). SIMNRA [36,37] (version 7.02) was used to simulate the measured RBS spectra and MultiSimNRA [38] was used to derive the oxygen areal density from the best fit to all energy spectra for each sample. Determining with RBS the areal density of a light element in a heavy substrate is only reflected indirectly as a "lack of W signal intensity" (for a more detailed discussion see in [21]). Therefore, samples with an oxide thickness of 15 nm or below cannot be quantified by this method. Furthermore, after TDS the roughness of the oxide film increased strongly, so that a quantification of the oxygen depth profile with RBS was no longer possible.

In addition to RBS, the nuclear reaction $^{16}O(^3He,p_0)^{18}F$ was used to directly measure and quantify the oxygen areal density in the surface oxide films. This method works for all samples, before and after TDS. To this end, the background-subtracted integral of the proton peak is taken and compared with SIMNRA [36,37] simulations. For the latter, the cross section data from Guitart Corominas and Schwarz-Selinger was taken [39].The used method is described in detail in [21] and yields a reliable measurement of the oxygen areal density in the whole oxide film.

3.7. D depth profiling

Nuclear reaction analysis (NRA) was applied to determine the depth-resolved concentration profile of D [40] in each sample. This was done after each experimental step (plasma loading, oxidation, TDS). The NRA measurements were performed *ex situ*, after the sample was carried

through air. To quantify D, the nuclear reaction D(^{3}He,p)α was exploited. By using ten different incident ^{3}He ion energies, ranging from 500 to 4500 keV, one can infer the D concentration in the sample to a depth of up to 7.4 μm. This fully covers the interesting regions of the sample, i.e., the surface oxide film and the 2.3 μm of self-damaged W that governs the D retention. A detailed description of the detector setup and the energy calibration can be found in [21].

The depth resolution of NRA measurements depends on the stopping power of the involved particles in the material. Since the density of the W oxide film (7.16 g/cm^3 [41]) is much smaller than that of pure W (19.25 g/cm^3 [42]) the depth resolution in the WO_3 oxide film is lower than in pure W. For the given setup, the depth resolution at the surface is 54 nm for pure W or 80 nm for WO_3. All depth resolutions were calculated with the program ResolNRA [43] using SRIM stopping powers [44].

For ^{3}He energies below 1200 keV, the α-particles from the D(^{3}He,α)p nuclear reaction can contribute information about the D concentration in the near surface region to a depth of a few hundred nanometers, i.e., deeper than the oxide film thickness. As the stopping power of α-particles in W or W oxide is higher than that of protons, this method also provides a better depth resolution of 27.5 nm (pure W) or 50 nm (W oxide).

The programs SIMNRA [36] and NRADC [45] were used to deconvolute the D spectra of the different ^{3}He energies for quantitative D depth profiling. NRADC uses the proton and α spectra at all measured energies as input to construct the most likely distribution of D atoms across the sample depth. A detailed description is given in Ref. [45]. The cross section data from Besenbacher and Möller [46] was used for the α spectrum and the cross section data from Wielunska et al. [47] was used for the proton spectra. Both cross section measurements have a total uncertainty of $< \pm 5$ %, which determines the systematic uncertainty for the absolute quantification of the D areal density. The accuracy of the ion beam current measurement is typically within 3–5 % and together with the statistical error of approximately 1 % (depending on the ion dose, ion energy and D concentration in the sample). Thus, the reproducibility of the NRA measurements also stays within 5 % relative to each other.

4. Results and discussion

4.1. Effects of high temperature (1000 K) exposure on electro-chemically grown W oxide films

In order to quantify the effect that the outgassing D has on the oxide film, it is necessary to separate D-induced changes from thermally induced changes during the heating ramp in TDS. Therefore, we studied the effect of temperature on thermally and electro-chemically grown W oxide films without D being present. To this end, we have investigated the changes that a 3 K/min ramp to 1000 K and holding the sample for 3 h at this temperature induces in the oxide films of batch 3 (see Tab. 1) via SEM imaging and NRA measurement of the oxygen areal density. The samples from this third batch were only polished and oxidized but not self-damaged or D filled.

4.1.1. SEM imaging:

In Fig. 3, SEM images of a 40 nm thick, electro-chemically grown W surface oxide are shown before and after a 3 K/min ramp to 1000 K and holding the sample for 3 h at this temperature. The images have the same magnification and show two different spots on the same sample. Images a) and b) show the oxide before and after the heat treatment, respectively. Both images are taken in secondary electron (SE) mode.

In image a), before the temperature treatment, four different W grains can be seen. The grain boundaries are clearly visible. All grains are covered by a homogeneous, smooth oxide film. This is as expected for the electrochemical oxidized sample (see Section 3.4). After annealing to 1000 K, (b), the sample shows a crystalline-like, striped surface structure. We interpret this as a temperature-induced transformation of the originally amorphous electro-chemical oxide to a nanocrystalline oxide that is reported in literature to take place at temperatures above 660 K [48]. Furthermore, small cracks form on some isolated spots in the oxide film. The SEM image in Fig. 3 b) is taken in SE mode and the edges of these cracks thus appear bright. In some cases, the cracks are wider and enclose small areas that appear to be depressions. It appears likely that in these cases small portions of the metallic W surface lie uncovered. Examples for these areas are marked by the arrows in Fig. 3 b).

The same trend is visible for a thinner 20 nm thick electrochemically grown oxide. The corresponding SEM images are shown in the Supplementary material S1. It should, however, be noted that the thin (20 nm) electro-chemical oxide shows more small areas where the oxide film has de-laminated and the metallic W is visible compared with the thicker (40 nm) film shown in Fig. 3. Nevertheless, also there the oxide film is mostly still intact. For comparison, also a 30 nm thick thermally grown oxide film has been studied (images in supplementary material S1). There the oxide film is mostly intact and only small regions with snowflake-like cracks in the oxide film are visible after heating.

4.1.2. NRA

The results of the NRA measurement of the oxide areal densities before and after the high temperature exposure are listed in Table 1. They show no or only a very minor loss of oxygen for the thick (40 nm) electro-chemically grown oxide and for the thermally grown oxide (33 nm). For the thin (20 nm), electro-chemically grown oxide, the oxygen loss in the order of 10%, which is in accordance with the SEM images

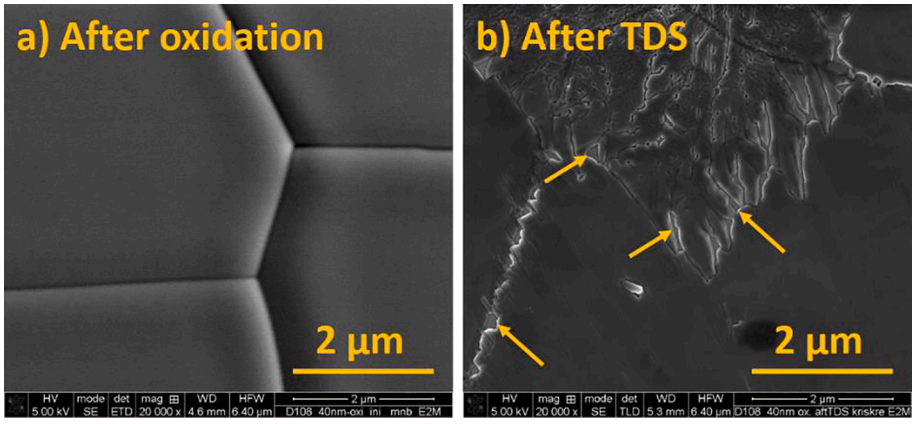

Fig. 3. SEM images of a D-free W sample with a 40 nm thick electro-chemically grown W oxide film. a) directly after oxidation, b) after exposure to the same TDS procedure (3 K/min temperature ramp to 1000 K in vacuum) that was used for the D-containing samples. Both images are taken in SE mode.

Table 1
Oxygen areal density of the D-free W samples before and after exposure to 1000 K during TDS.

Sample	Oxygen areal density (10^{15} O atoms/cm^2)			
	As grown	After 1000 K	Difference	Difference (%)
20 nm electro-chem. ox.	117.9 ± 2.8	104.4 ± 2.7	13.5 ± 3.9	12 ± 4
40 nm electro-chem. ox.	226.8 ± 3.5	221.0 ± 3.5	5.8 ± 5.0	2.5 ± 2.2
30 nm thermal ox.	163.8 ± 3.1	166.8 ± 3.2	−3.0 ± 4.5	−1.8 ± 2.8

(see supplementary S1). This confirms that up to 1000 K, the oxygen amount on the samples is (mostly) stable and no or only small amounts of oxygen are lost due to, e.g., evaporation of WOx molecules.

4.2. Deuterium depth profiles

This part focuses on the evaluation of the D depth profiles that were obtained by NRA in chronological order of the experimental steps. For each measurement, a different spot on the sample was chosen to exclude ion-beam induced effects on later measurements. The profiles are shown for one representative sample with an oxide thickness of 100 nm, but all other samples behave in the same fashion. Details for the D depth profiling technique with NRA are described in Section 3.7. The error bars that are shown in the D depth profiles in Fig. 4 stem from a Markov-Chain Monte Carlo post processing calculation (see [49]). However, one has to keep in mind that the total error of the measurement is in reality higher, as described in section 3.7.

The first D depth profile is determined after D loading with the low-temperature D plasma. It is represented by the black line in Fig. 4. The D concentration is determined by the damage profile, which is represented by the grey dashed line (with units on the right *y*-axis). Note that the D retention saturates above a certain damage level [6] and is thus flat topped. Therefore, this shape of the D retention is expected and coincides nicely with measurements performed in the past on samples treated in the very same manner [9]. The D concentration in the self-damaged zone is about 1.6 at.%. The total areal density of D in this sample is 1.96 × 10^{17} D/cm^2. Furthermore, it is evident that the D concentration in the bulk W is negligible in comparison to the D concentration in the self-damaged zone.

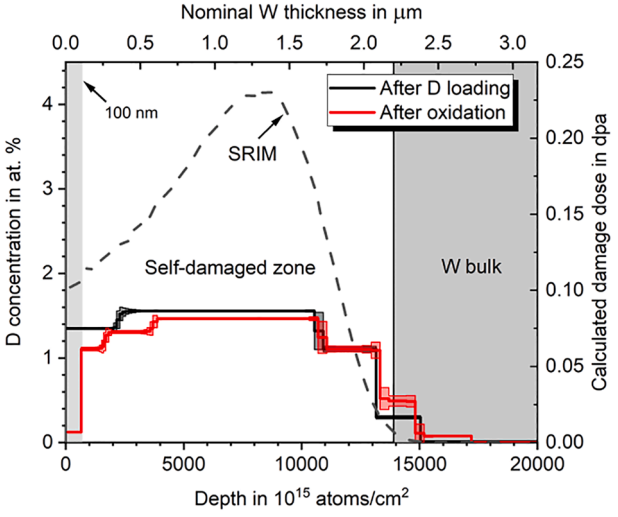

Fig. 4. D depth profiles of a 100 nm thick electro-chemically grown oxide after plasma exposure (black line) and after oxidation (red line). The D depth profiles are almost identical. The oxidation only lowers the D concentration in the oxide film itself (indicated by the light grey background area close to the surface), but does not alter the D profile in the underlying self-damaged W. The lower x-axis shows the areal density as derived from NRADC. The upper x-axis was derived by converting the areal density into a thickness value (assuming a W oxide density of 7.26 g/cm^3 and W bulk density of 19.25 g/cm^3). The dashed grey line shows the calculated damage profile in dpa according to SRIM (units on the right y-axis). The gray area on the right marks the un-damaged bulk W. (For interpretation of the references to color in this figure legend, the reader is referred to the web version of this article.)

The red line in Fig. 4 represents the D profile measured after the electro-chemical oxidation. In the self-damaged zone, it coincides very well with the previous profile (black line), indicating that the D remains trapped in the defects there. However, at the surface where W is converted to W oxide (indicated by the light grey background area), the D concentration is significantly lower (0.14 at.%) than the first (black) D profile. This shows that (most of) the trapped D, is released from W that is converted to oxide. The total amount of D that is still in the sample (1.97 × 10^{17} D/cm^2) remains, however, unchanged within the measurement uncertainty. Thus, the fraction of D that is released during oxidation is negligible. It is also noteworthy to mention that the coloration of the oxide film after oxidation matches the expected interference color for hydrogen-isotope-free WO_3. If there were D (or H atoms from the oxidation solution) in the oxide, D-W-bronze would form and lead to a visible color change of the film ([21,50]).

A third NRA measurement was performed after the 1000 K TDS exposure for all samples. In all cases, the D was completely released during TDS and there was no D detectable with NRA.

4.3. TDS results

4.3.1. QMS signals of the natural and 100 nm oxide sample:

To illustrate the effects that oxide films have on TDS spectra, we first compare a sample with natural oxide (reference) with a sample with 100 nm thick oxide. Fig. 5 a) shows the background subtracted QMS signals of mass channel 3 (HD) and mass channel 4 (D_2) (left *y*-axis) as function of time for the natural oxide (black lines) and the 100 nm thick oxide (red lines). The thin grey line (units on the right *y*-axis) shows the

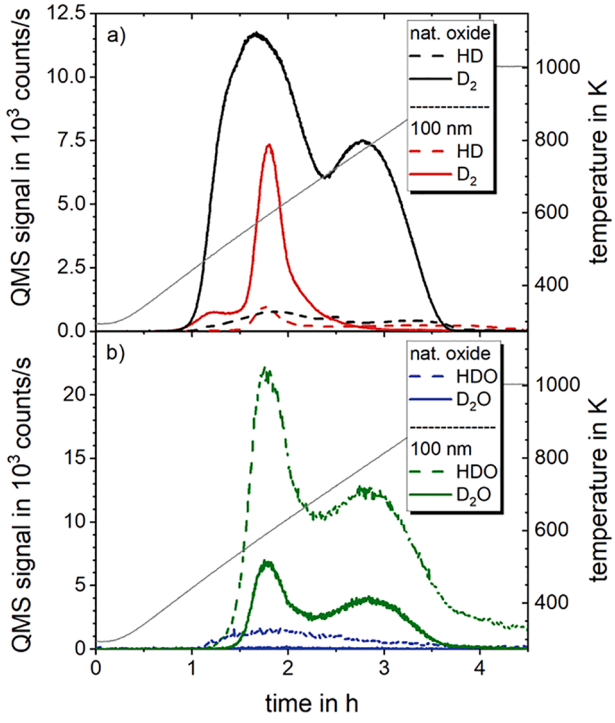

Fig. 5. Background-corrected QMS signals during the 3 K/min ramp to 1000 K of natural oxide and 100 nm thick oxide. a) D_2 and HD signal. b) HDO and D_2O signal. The temperature ramp is indicated in gray with units on the right axis.

temperature ramp. The signal for the natural oxide sample (thick black line) shows two distinct peaks, which nicely coincides with previous studies of such samples [9,16,17]. The onset of D release occurs at 410 K. This is as expected, since the samples were plasma-loaded at a sample temperature of 370 K, which means that traps (with low de-trapping energy) that can release D at this temperature have already done so during the loading. However, by comparing this with the signal of the 100 nm thick oxide sample (red lines), one sees a big difference in the release behaviour. The HD and D_2 signals seem to be strongly diminished for the oxidized sample, especially for high temperatures. The D_2 signal of the 100 nm oxide sample, the onset of the left flank of the first peak starts at the same temperature of roughly 410 K as for the natural oxide, but then stops rising and stays constant at a low level from a temperature of 475 K until it suddenly increases at T = 540 K. The peak of the oxidized sample (red) is reached at T = 595 K, which is at a slightly higher temperature than the peak maximum for the natural oxide sample (black line). Its height is still much lower than for the natural oxide case. The signal then strongly decays with temperature and stays far below the natural oxide signal until it vanishes at about T = 825 K. Especially, the second D_2 peak (which is measured for the natural oxide sample at T = 770 K) is not visible at all for the oxidized sample. Integrating over time, there are about 80 % less D_2 counts for the 100 nm oxide than for the natural oxide sample. HD behaves qualitatively similar as D_2 just on a much lower signal level.

This shows that the presence of an (100 nm thick) oxide film on the surface has a strong influence on the D release from W. Furthermore, since we know from the NRA D depth profiling that all D is released from the sample after TDS to 1000 K, this result immediately poses the question what happened to the remaining D (that is not released as D_2 or HD).

Fig. 5 b) gives a possible answer to this question. It shows the QMS signals of mass channels 19 (HDO) and 20 (D_2O) for these two samples. For the natural oxide sample there is virtually no D_2O detectable and only small amounts of HDO are present. For the oxidized sample, this is clearly different. There are strong signals for HDO and D_2O. Furthermore, these heavy water signals again show two clear peaks, as was the case for the D_2 release from the natural oxide sample. The first notable increase of the heavy water signal is measured at a temperature of 475 K, which coincides with the start of the plateau phase of the D_2 signal. The first peak from the heavy water signal is reached at about the same temperature as the first D_2 peak. The second peak, lies at the same temperature of 770 K for both samples although it now consists only of heavy water instead of D_2 or HD. This clearly indicates that released D interacts with the oxide film and is converted to heavy water species during the release process. Note however, that in Fig. 5 only background subtracted QMS counts are shown and the results are so far only qualitative. Please note further that no significant contribution was detected in any of the other measured mass channels.

To further our understanding of this conversion mechanism a quantification of the heavy water amount is necessary. However, calibrating and hence quantifying water molecule fluxes is typically not possible or requires at least a special setup, as these molecules can stick onto the chamber walls on their way to the QMS [51]. However, because the total amount of deuterium in the samples is known from NRA, the calibration factor for water can be derived by closing the deuterium particle balance. Details of this procedure are beyond the scope of this publication and will be published in a forthcoming paper [35]. Based on these calibration factors in the following absolute fluxes of D/s in the form of D_2, HD, HDO, and D_2O will be discussed.

4.3.2. Reactions of outgassing D with oxide and production of heavy water:

To illustrate the reaction of outgassing D with the oxygen in the oxide film we have a closer look at the absolute fluxes of desorbing heavy water. Fig. 6 shows the calibrated fluxes in D-atoms/s for: 1) D-containing molecules without oxygen (the sum of HD + D_2, solid lines) and 2) heavy water molecules (the sum of HDO + D_2O, dashed lines) for

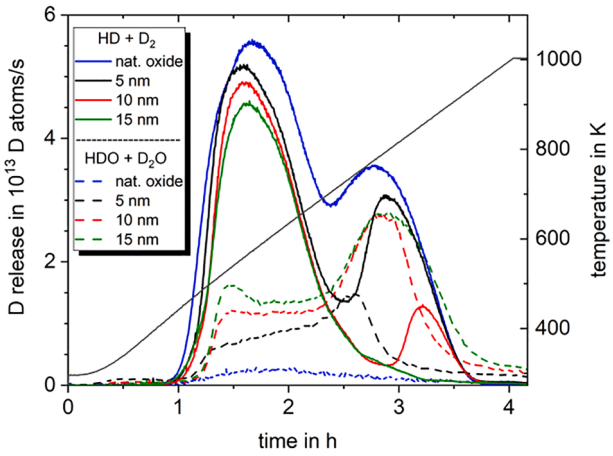

Fig. 6. Quantified D release in form of deuterated hydrogen (D_2 + HD; solid lines) and heavy water (HDO + D_2O; dashed lines) for the thin oxide samples with varying thickness of the oxide film.

small oxide thicknesses up to 15 nm. For comparison, the natural oxide sample is included (blue lines). The grey solid line (units on the right *y*-axis) shows the temperature, which was ramped with 3 K min^{-1} to 1000 K. When looking at the sum of the HD and D_2 desorption, a small shift to higher temperatures of the low-temperature flank of the first peak is visible, which indicates a time delay of the D release. Furthermore, one can see that D release in form of heavy water molecules already sets in during the low-temperature peak at about 490 K and forms a sharp step-like rise, followed by a relatively constant plateau throughout the first peak (to about 700 K). The height of the heavy water flux of the plateau increases with increasing oxide thickness. For the natural oxide, no such feature is visible. Hence, these signals do not stem from reactions of desorbing deuterium with the chamber walls but directly from the samples. This clearly shows that already at relatively low temperatures (490 K) the outgassing D chemically reacts with the oxide film and produces heavy water or precursors for it.

The behavior of the second peak is, however, even more curious. There, the sum of the HD and D_2 desorption shows a clear peak for the natural oxide (solid blue line) which becomes smaller with increasing oxide thickness until it completely vanishes for the 15 nm thick oxide (green solid line). As we know from the discussion above that D is already thermally de-trapped from the defects in the self-damaged W at these temperatures, the D that is "missing" from the HD and D_2 desorption flux of the second peak has to be released in form of other volatile species, i.e., heavy water molecules. And indeed, the dashed lines which represent the heavy water molecules show a rise whenever the HD + D_2 signal in the second peak is lower than expected from the natural oxide. The green lines (15 nm oxide) clearly show that for higher temperatures D is released almost exclusively as heavy water. In this case, the oxide film is thick enough to supply enough oxygen to interact with all released D. The situation changes for the 10 nm thick oxide (red lines). Here, we can see a drop in the heavy water signal roughly in the middle of the high temperature peak. This drop is accompanied by an increase in HD and D_2 desorption, which indicates that the oxide on the surface has been fully reduced to heavy water species and released into vacuum. For the 5 nm thick oxide (black lines) this effect is even more pronounced and the changeover sets in earlier (at a lower temperature), as less oxygen is available.

The observation that the HD + D_2 signal rises again only after all oxygen in the oxide film is consumed is supported by the SEM images of the sample surface after TDS that are discussed in Fig. 7. For the originally 5 and 10 nm thick oxide films in Fig. 7 a) and b), the oxide is completely removed from the surface. For the originally 15 nm thick oxide film in Fig. 7 c), however, some oxide is remaining on the surface. This is in agreement with the interpretation of the TDS spectra for this

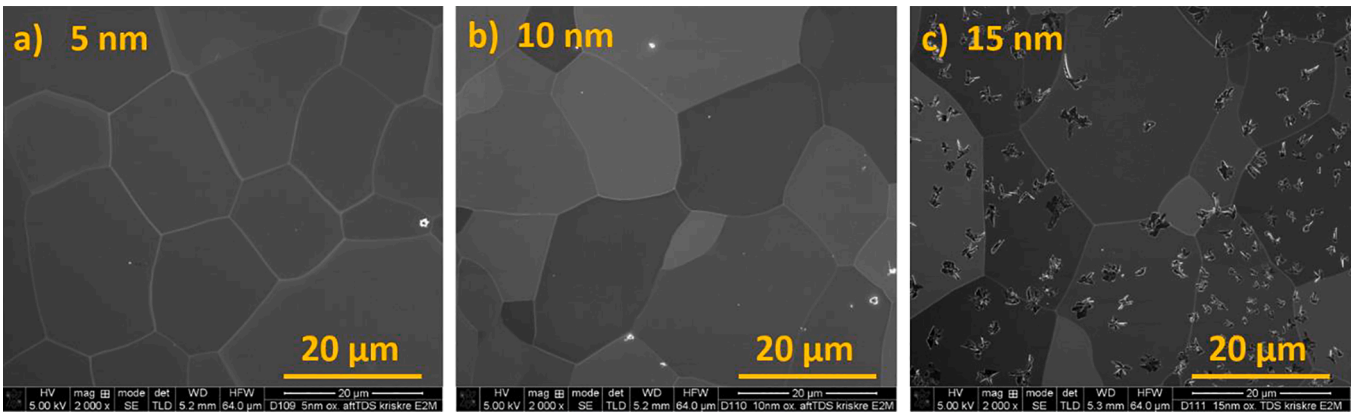

Fig. 7. SEM images in SE mode of the second batch of self-damaged, D loaded and electro-chemically oxidized W samples after D release during TDS up to 1000 K. In image a) and b), the thin surface oxide film (originally 5 or 10 nm, respectively) is completely removed. In c), some remnants of the originally 15 nm thick oxide film remain. They are distributed like small islands on the otherwise clean W surface.

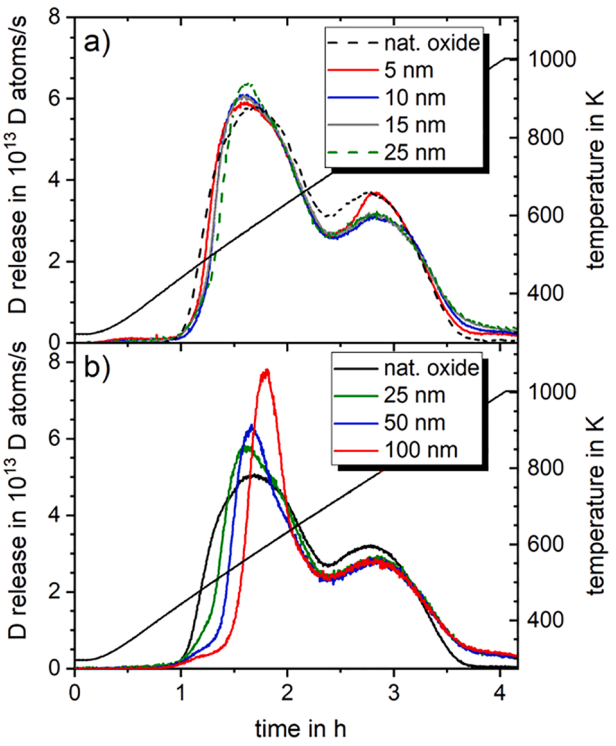

Fig. 8. Total D release. a) thin oxide films of 5 – 25 nm b) thicker oxide films of 25 – 100 nm. The natural oxide signal is shown in both graphs for comparison. In a) the signals for the natural oxide and the 25 nm thick oxide are scaled by a factor of 1.15 to match the D content of the other samples shown in a). See text for details. The solid grey line shows temperature (right y-axis).

sample, where heavy water production continues until all D is released from the sample. Obviously, all D stored in the self-damaged zone underneath the oxide was completely released before all oxygen in the oxide film was converted to heavy water.

It is interesting that the remaining oxide in Fig. 7 c) is not distributed homogeneously across the W surface, but is clustered in small islands on an otherwise oxide free W surface. Note that also for this "oxide free" surfaces it might be possible that the last one to two monolayers of oxygen are more strongly bound than the rest of the oxide and thus might remain on the surface, even during D release at high temperatures. Therefore, when we speak of "oxide free" or "clean" surfaces, we only refer to oxide films thicker than one or two monolayers. Please also note that for SEM imaging, the samples were carried through air and thus a natural oxide film (invisible in the SEM images) has re-formed on the sample surface. The oxide islands visible in Fig. 7 c) cover a much smaller fraction of the surface area than the clean W. However, the dominant release channel of D towards the end of this TDS run was still heavy water (HDO, D_2O). This observation indicates that although most of the D reaches the surface at a spot where the oxide was already removed, the D atoms diffuse across the surface until they reach an oxide island where they form heavy water before being released. The average distance between two neighboring oxide islands is in the range of several µm to several 10 µm, which means that a D atom diffuses on average at least 1–10 µm across the surface before it reaches an oxide island. This indicates a high mobility of D atoms on the sample surface. It should be noted that D atoms that reach the surface cannot immediately desorb, but have to find another D atom and recombine to a D_2 molecule before they can be released as molecule. As we see only minor contribution of D_2 in the D release, as long as oxide is still present, this means that the mean free path of D on the W surface is greater than 1–10 µm before it meets another D atom. This also indicates that D that reaches an oxide island is bound there and remains until a second D atom reaches the spot and forms a water molecule that is then released.

Furthermore, the results in this section allow an estimation of when surface oxides becomes relevant for D release signals in TDS in general. As heavy water quantification in TDS is very difficult, the D_2 and HD signal is often the only one that can be evaluated quantitatively. Therefore, it is important to estimate, at which quantity surface oxide films significantly influence the release spectra of these two mass channels. From Fig. 6 it is obvious that even the 5 nm thick oxide film significantly alters the D_2 + HD spectra in our case (especially the position and magnitude of the high temperature peak). For the natural oxide, on the other hand, the ratio of heavy water signal to D_2 + HD signal is negligibly small and we can thus assume that the outgassing behaviour is not strongly affected. However, it is important to keep in mind that in this present study we used self-damaged W, which has a D retention that is orders of magnitude higher than for un-damaged W. Thus for experiments that use un-damaged W, even the small amounts of oxygen in the natural oxide film could influence the D release. To estimate the influence of oxide films in such cases, it makes sense to look at the ratio of D atoms stored in the sample to oxygen atoms in the oxide film. Considering the SEM images in Fig. 7 a) and b), we see that the oxide can be completely removed by outgassing D, if enough D is available. Thus, it is reasonable to assume that the ratio of O to D atoms in the sample is the decisive quantity that determines if the oxide film influences the D release. In our case, the total amount of D that was retained in the self-damaged W as measured by NRA is 2.3×10^{17} D/cm^2 for the samples with thin oxide (5, 10, 15 nm) and 2.0×10^{17} D/cm^2 for the natural oxide reference sample. The amount of oxygen (also

measured by NRA) in these samples and the ratio of O/D is given in Table 2. In case of the natural oxide, the oxygen amount is in the order of 8 monolayers. The ratio of oxygen and deuterium is hence 4.2 %. If one assumes that the last one to two monolayers may be more strongly bound than the rest, they might not be easily accessible to reduction by D. In this case the ratio of oxygen that is accessible for reduction to D would be even lower (3.2 ± 0.5 %). By comparing the O/D ratio in Table 2 with the D release spectra in Fig. 6, it becomes evident that for O/D ratios of < 10 % (5 nm thick oxide) the oxide film already strongly affects the D release spectra. If the O/D ratio is greater than 30 % (15 nm thick oxide), the D release spectra is completely dominated by the oxide film in the sense that the second (high) temperature peak vanishes completely in the D_2 + HD signals.

4.3.3. Comparison of the total D release for all different oxide film thicknesses (5 to 100 nm):

We have seen that surface oxide films can alter the molecular species in which D is released from W. However, in order to asses if an oxide film affects also the release temperature of D (and thus the determination of binding energies of D in W defects), a comparison of the total D flux is necessary. Fig. 8 shows this total D flux derived by summing up the quantified contributions from HD, D_2, HDO and D_2O for samples with different oxide thickness.

Fig. 8 a) shows the samples with thin oxide films (second batch) of 5 nm (red line), 10 nm (blue line) and 15 nm (grey line). Additionally, it also shows the natural oxide reference sample and the 25 nm oxide film from the first batch (black and green dashed line, respectively) to allow a direct comparison of the different thickness regimes. Note that the signals from the natural oxide and the 25 nm thick oxide (batch 1) have been scaled by a factor of 1.15 in Fig. 8 a) to match the higher D content in the samples with thin oxides (batch 2), as described in Section 3.3. It is immediately obvious that the total D release of all samples has remarkably similar peak shapes. The sum spectra in Fig. 8a) show two distinct peaks for all different oxide thicknesses, i.e., the total D release spectrum matches the expected general shape of the release in form of HD + D_2 of the natural oxide sample. However, a slight difference between the different samples is visible. With increasing oxide thickness, the left flank of the first peak slightly shifts to higher temperatures.

Fig. 8 b) presents the total D flux from samples of the first batch, i.e., natural oxide (black line), 25 nm (green line), 50 nm (blue line) and 100 nm (red line) thick oxide. For these thicker oxide films, the shift of the first peak is much more pronounced than for the thinner ones. The first peak maximum shifts from 560 K for the natural oxide to 590 K for the 100 nm thick oxide. It is worth mentioning that the release of D from trapping sites in the self-damaged zone is thermally activated and thus is not affected by the oxide film on top of the self-damaged film. This means that D is released from the traps in the self-damaged layer in the same fashion as for the sample with natural oxide. The peak shift in the release spectrum of the sample with (thick) oxide films thus shows that the oxide films delay the D on its way to the sample surface. As the oxide film itself shows a high D retention at temperatures around 500 K (see Fig. 13 in Section 4.4) delay can be explained at least in part by re-trapping of D in the oxide film. This indicates that only after all trapping sites in the oxide are filled with D, the D that is released from the self-damaged layer can pass through the oxide and reach the surface. The oxide film thus acts as a sink or reservoir for outgassing D.

However, we would like to mention already at this point that the ramp-&-hold experiments, which are discussed in the next section (4.4), indicate that the oxide film acts not only as a sink for D but also as an transport barrier that reduces D release from the sample even after the oxide is filled with D.

Furthermore, with increasing oxide thickness, the first peak becomes narrower but higher and the amount of D that is released in the first peak decreases slightly. The first peak contains 63 % of the total D release from the sample for the natural oxide, 59 % for the 25 nm, 56 %, for the 50 nm and 53 % for the 100 nm thick oxide. The shift of the peak position and the change of the quantity of released D in the two peaks shows that in this case also the calculation of binding energies of D in defects in W (that can be derived from such TDS spectra) would be affected by the oxide film.

However, when using self-damaged W and samples with only natural oxide (as is the case for experiments for the determination of D trapping energies in displacement-damaged W), the amount of stored D is very large compared with the amount of oxygen in the oxide film. Consequently, the natural oxide film will be reduced early on by the first outgassing D, which means that heavy water formation will play only a minor role and the expected peak shift due to the oxide will be very small. Thus, we can assume that the natural oxide will not significantly influence the D release behaviour from W in these cases. For experiments with un-damaged W with only few defects, however, even the natural oxide may significantly influence the positions and relative quantities of D release during TDS even when considering heavy water as an additional release channel for D (as in Fig. 8). Thus, even the natural oxide may influence the determination of binding energies of D in material defects in these cases.

The second (high-temperature) peak has a very similar shape and position for all samples; only the natural oxide shows a slightly higher maximum at slightly lower temperatures (770 K instead of 785 K). Furthermore, for the high-temperature side of the second peak, the curve of the natural oxide (black) falls off strongly, whereas the curves of the oxidized samples decay slower. The D signals of the oxidized samples surpass the black curve at about 3.3 h and thus the D release has a high temperature tail in these cases. We attribute this effect to the "wall sticking" of heavy water molecules that are released by the oxidized samples. In contrast to the natural oxide (where almost no heavy water is formed), this leads to a delayed signal as heavy water is repeatedly adsorbed and released from the chamber walls before it reaches the QMS.

4.3.4. Oxide film changes after D release:

Fig. 9 shows SEM images of the thicker oxide films (25, 50 and 100 nm) after D release during TDS up to 1000 K. The surface morphology of the oxide films is changed drastically by the outgassing D. In the case of the 25 nm thick oxide film (Fig. 9 a)), snowflake-like structures are visible on top of a smooth surface. The elemental composition of the sample surface was checked with energy-dispersive X-ray (EDX) mapping, which is shown in Fig. 10 for a different spot on the same sample. There, it is clearly visible that the snowflake-like structure represents the remaining W oxide while the area in between consists of smooth, oxide-free W. This shows that the reduction of the oxide film is not a homogeneous process but leads to two-dimensional modifications of the film. Please note that the different grey scales of the metallic W surface are caused by two different W grains that are visible in Fig. 9 a).

When starting with thicker oxide films (50 and 100 nm) in Fig. 9 b) and c) the surface is still (mostly) covered by the oxide film. Nevertheless, the film shows strong modification of either columnar crystal structures or coral-like structures. Comparing these images to the annealed D-free reference sample shown in Fig. 3 b), it is obvious that the changes during D outgassing far surpasses those of the solely temperature-induced oxide modification.

It is also interesting to take a closer look to the region at the edge of the self-damaged zone, where the sample has been shielded by the Mo mask during the W ion bombardment. SEM images of the edge

Table 2
Ratio of oxygen to D for different oxide thicknesses.

Oxide thickness in nm	O amount in 10^{15} atoms/cm^2	O/D ratio in %
natural oxide	8.4 ± 1.1	4.2 ± 0.5
5	30.0 ± 1.4	13 ± 0.7
10	59.8 ± 1.9	26 ± 0.9
15	84.4 ± 2.2	37 ± 1.0

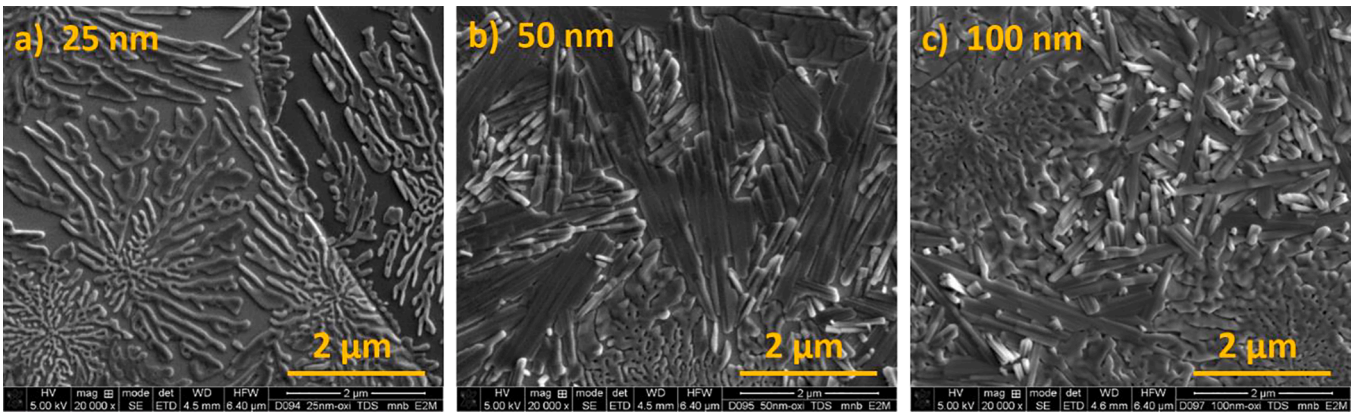

Fig. 9. SEM images of the first batch of self-damaged, D loaded and electro-chemically oxidized samples after D release during TDS up to 1000 K taken in SE mode with identical magnification.

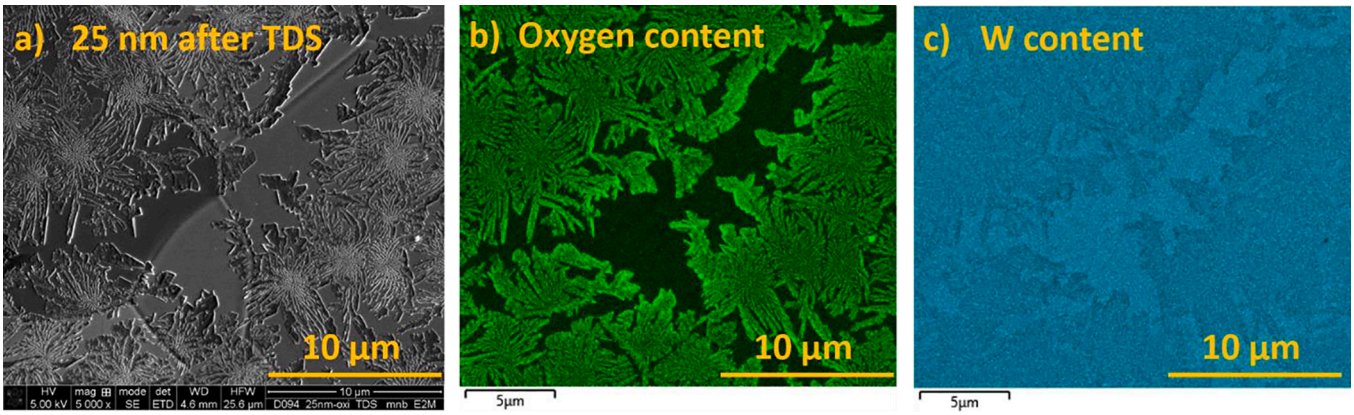

Fig. 10. Energy-dispersive-X-ray (EDX) mapping of the 25 nm thick oxide film after TDS. a) SEM image in SE contrast, b) oxygen signal and c) W concentration.

separating the damaged and un-damaged zones are shown in Fig. 11. The borderline between the two zones is clearly visible in Fig. 11 a) and b). In the D-containing damaged zone most of the oxide film is removed, as discussed above. However, in the un-damaged zone the oxide film is still mostly intact and covers the surface area almost completely. The film still shows some modification that goes slightly beyond the alteration that one would expect from the high temperature exposure (without D) alone. This is the case because even in the annealed and un-damaged W some small amount of D is retained during the plasma exposure. The quantity of D is, however, too small to cause significant removal of this 15 nm thin oxide film. The situation changes when looking at the edge region of the originally 5 nm thick oxide film that is shown in Fig. 12. Here even in the un-damaged zone the oxide film is removed from most of the surface area. When comparing this to a 1–2 nm thick natural oxide film, this result might indicate that the amount of D stored in an un-damaged and annealed (2000 K) W sample is just

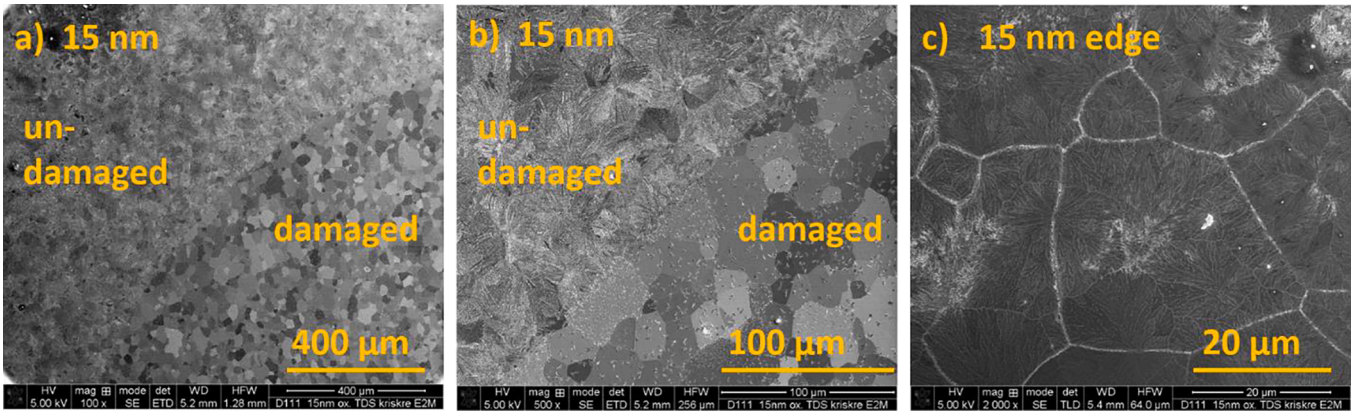

Fig. 11. SEM images in SE mode of the edge of the self-damaged zone for the originally 15 nm thick oxide film after TDS (round edge is due to the shape of the mask holding the sample). a) Overview over the edge region, where the top left is not self-damaged and thus the W underneath the oxide contains only little D. b) Same with higher magnification. The edge between the two regions is clearly visible. In the undamaged part, a closed oxide film is retained after TDS. c) A magnified image of the un-damaged zone. The oxide is only partially eroded by outgassing D, since the D amount underneath was much smaller in this region.

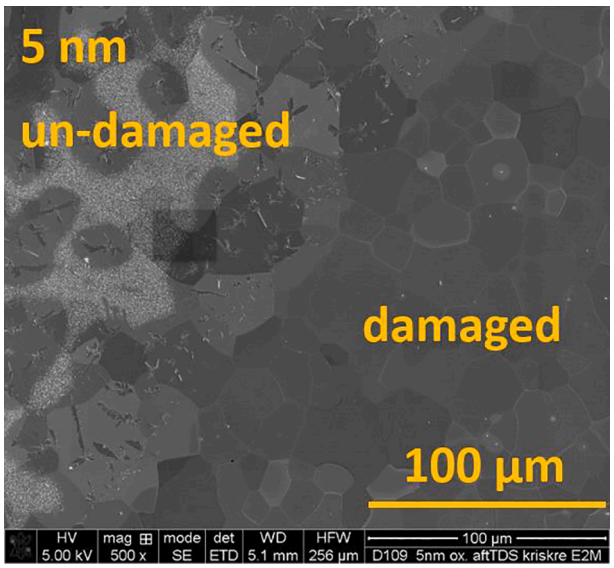

Fig. 12. SEM image of the edge of the originally 5 nm thick oxide film. The oxide is removed completely above the damaged area and only partially removed above the undamaged area.

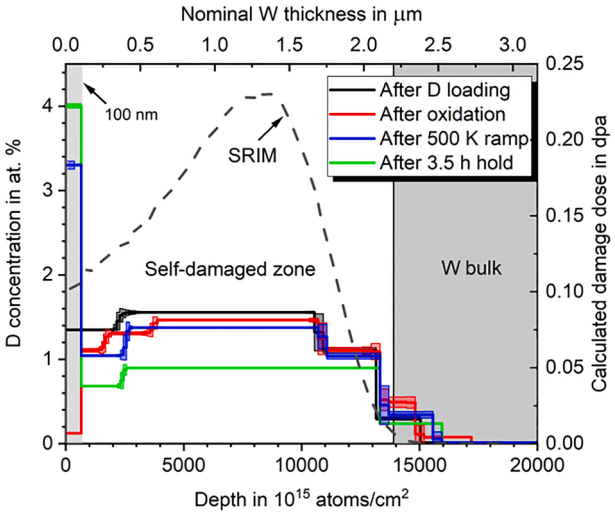

Fig. 13. D depth profiles of a 100 nm thick electro-chemically grown oxide after a 3 K/min ramp to 500 K (blue line) and after a second ramp to 500 K and a 3.5 h hold (green line). The gray dashed lines shows the calculated damage profile in dpa according to SRIM (units one the right y-axis). For comparison the depth profiles before TDS are also shown (black and red line). (For interpretation of the references to color in this figure legend, the reader is referred to the web version of this article.)

enough to remove the natural oxide film during TDS completely. This indicates that for laboratory experiments with an un-damaged W even the natural oxide film may have a significant influence on TDS spectra.

4.4. Ramp-and-hold experiments to 500 K

In order to study the before-mentioned transport barrier effect of the oxide film further, the D release from one additional sample with 100 nm thick oxide from the first batch was studied by TDS. The sample was first ramped with 3 K/min to 500 K and then cooled down immediately by retracting the oven. Afterwards, it was exposed to a second ramp to 500 K and held at this temperature for 3.5 h. This temperature was chosen as D_2 desorption shows a peculiar plateau starting at this temperature (see Fig. 5 a)). As mentioned before (see discussion of Fig. 5 b)) this temperature is just slightly above the temperature where the production of heavy water sets in (at roughly 475 K). This ramp-&-hold experiment thus aimed to study how D is transported through the oxide film at this reduced temperature and how the film is modified by the outgassing D and heavy water production in this case.

4.4.1. D depth profiles and O content:

The D depth profile after the first heating ramp to 500 K is shown in Fig. 13 as blue line. For comparison the D depth before TDS (black and red) are also shown. As is evident from Fig. 13 there is an accumulation of deuterium in the oxide film after the ramp. Analysis of the depth profile yields that about 11 % (0.22×10^{17} D/cm^2) of the D originally retained in the sample (1.97×10^{17} D/cm^2) was transferred from the self-damaged zone to the oxide film. Assuming a constant D concentration throughout the oxide film the local concentration of D in the oxide film is 3 at.%. The total D amount after the ramp is 1.93×10^{17} D/cm^2. Thus, only approximately 2 % of the D that was originally retained in the sample was released during the ramp.

After this first ramp and subsequent NRA measurement, the same sample was reinstalled in the TDS setup, was again ramped to 500 K and held at that temperature for 3.5 h. The deuterium depth profile after the holding period is represented by the green line in Fig. 13. A small additional amount of D was transferred from the bulk to the oxide film such that 13 % (0.26×10^{17} D/cm^2) of the originally retained D are trapped in the oxide film. The corresponding average D concentration in the oxide film is now at 4.0 at.%. The total D areal density of the oxide and the self-damaged layer underneath is 1.43×10^{17} D/cm^2. Thus another 25% of the originally retained D was released during the holding period. This is about eight times more than during the previous step (ramp only). In total 28 % of the retained D was released from the sample during these two experiments. Consequently, the D concentration in the damaged-region decreased from originally 1.6 at.% to 0.9 at.%. As the oxygen areal density (measured by NRA) changed only by a minor amount during these two experimental steps, it is reasonable to assume that the oxide thickness after the holding time is comparable to that after oxidation. As significant amounts of D (28 %) were released through the oxide film during the ramp-&-hold period, this indicates that the oxide is saturated with D and the maximum D concentration in the oxide (for 500 K) is reached.

4.4.2. Desorption spectra:

Fig. 14 a) and b) show the D_2 (red) and HDO (blue) desorption fluxes for ramp and hold experiments to 500 K. The temperature ramps are shown as straight black lines with units on the right *y*-axis. Fig. 14 a) shows the D_2 and HDO release for a sample with natural oxide that was ramped only once to 500 K and held there. Fig. 14b) shows the desorption of the sample with the 100 nm oxide that was ramped first to 500 K, cooled down and ramped again to be held at that temperature for 3.5 h. The color code is the same as in Fig. 14 b). However, the absolute scales for the desorption fluxes differ by a factor of 20. In both figures, the D_2 desorption fluxes of 'full' TDS spectra ramped up to 1000 K of identical samples are shown in grey for comparison. The two samples with the natural oxide stem from a previous study and underwent identical preparation as the samples from this study [9].

Comparing the D_2 desorption fluxes from the two samples in Fig. 14 a) with each other as well as the ones from the two samples from Fig. 14 b) one can see again the excellent reproducibility of the data. In both cases the initial D_2 desorption fluxes for the ramps to 500 K are identical to the 'full' TDS ramps. They only start to deviate above 500 K were the oven is either retracted or the temperature is held constant.

For the sample with the natural oxide (Fig. 14 a)), the D_2 desorption flux (red) shows a maximum, when the temperature of 500 K is reached and afterwards decays exponentially. This is expected, as the D release is governed by thermal de-trapping from material defects in the self-damaged W. At a given temperature only a limited amount of D can

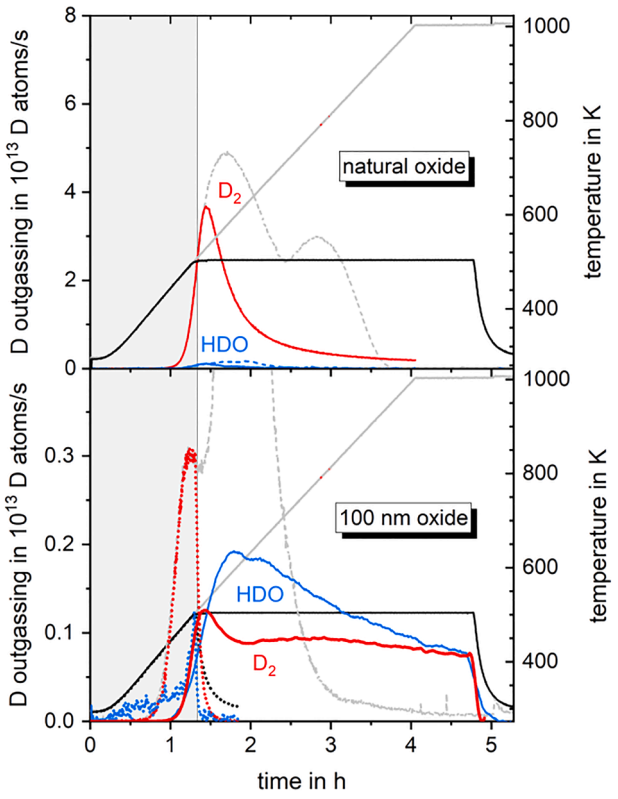

Fig. 14. D_2 (red) and HDO (blue) desorption from W during ramp-&-hold experiments to 500 K. a) shows a sample with natural oxide and b) shows a sample with 100 nm thick oxide. The temperature ramp to 500 K is shown in black for both cases. In b) the D release of the first ramp and the quick cool-down is shown with thick dotes lines; the D release for the ramp-&-hold phase is shown as thick solid lines. For identical samples also 'full' D_2 TDS spectra (solid grey lines) and their temperature ramps up to 1000 K (dashed grey lines) are shown for comparison. (For interpretation of the references to color in this figure legend, the reader is referred to the web version of this article.)

be accessed (de-trapped) and hence the signal has to drop exponentially. The maximum of the D_2 desorption flux for the ramp-&-hold at 500 K nearly reaches the maximum desorption flux of the "full" TDS spectrum (grey). The total D amount, which degassed during the ramp-&-hold in the form of D_2, HD and HDO was 9.4×10^{16} D atoms. This is about 36 % of the total D amount that was originally retained in the sample. It is also clearly visible that the natural oxide sample emits almost no heavy water, as could be expected from the investigations of the previous sections.

In contrast, the spectra of the 100 nm thick oxide (Fig. 14 b)), show differences compared with the ones of the natural oxide. First, the absolute D_2 flux is significantly lower in accordance with Fig. 5 a). Second, for the 100 nm oxide, a small heavy water contribution arises already during the ramp. Third the D_2 desorption flux shows a short dip at around 500 K that coincides with a strong rise of the heavy water production. This can in part be explained by the reservoir effect of the oxide which takes up significant amounts of D during the ramping phase (see section 4.2.) The total D amount, which degassed during the ramp in the form of D_2, HD and HDO until the oven was retracted is 4.2×10^{15} D atoms (no D_2O signal was measured), which agrees well with the D loss measured by NRA after the ramp (self-damaged area on sample : 1.4 cm^2).

For the holding phase of the 100 nm thick sample (solid red and blue lines in Fig. 14 b)), the shapes of the D release spectra look also very different. Firstly, the D_2 signal shows an initial peak after the second ramp reaches 500 K. This peak is probably due to D that was stored inside the oxide film after the first ramp (compare with the D depth profiles after the ramp in Fig. 13). More importantly, after that (during the holding phase) the desorption does not show the expected exponential decay of the D_2 signal, but a relatively constant plateau of about 1×10^{12} D/s. This plateau shows that a) the low-energy D traps in the self-damaged W are not depleted (yet) during the holding phase at 500 K and b) that the oxide film acts as a bottleneck for the D release. It seems to be the limiting factor for the D out-flux, which means that the oxide acts a transport barrier for D.

On the other hand, the deuterium released as HDO (blue), peaks about half an hour after the holding temperature of 500 K was reached and then drops continuously by about 60 % until the end of the holding phase. This indicates that over time less D reacts with the oxide to form heavy water. As the formation of HDO indicates that oxide is removed from the sample, we would expect that the transport barrier effect of the oxide decreases over time, which would cause an increase in the D_2 flux from the sample. The fact that the D_2 out-flux stays relatively constant could possibly be caused by the formation of channels through the oxide film through which the D can leave the sample without direct contact with the oxide. In other words, the bottleneck is expanding, which counteracts the decaying D out-flux. This hypothesis of channel formation is supported by the SEM images of the sample after the ramp-&-hold experiment, which also shows pinholes/channels in the oxide film (see Fig. 15 and Fig. 16).

4.4.3. SEM:

Fig. 15 shows SEM images of the surface of the 100 nm thick oxide film after the ramp-&-hold experiment to 500 K. The oxide film is still mostly intact, as can be expected from the NRA measurements and TDS spectra that showed only comparatively little oxygen loss. However, across the surface many small "hole-" or "bubble-like" structures are visible (see Fig. 15 a)). They are distributed uniformly across the sample, but appear to be more frequent along grain boundaries. In Fig. 15 b) and c) a magnified image of these features is shown in SE and back-scattered-electron (BSE) contrast, respectively. Here, the features appear to be small bubbles that are burst open towards the surface. Especially in Fig. 15c) it becomes apparent that the hole itself is surrounded by a larger area that corresponds to the larger diameter of the underlying bubble (compare Fig. 16b)). For clarification it should be mentioned that the dark circles in Fig. 15a) resemble the diameter of the underlying bubble and that the actual open holes are much smaller in diameter than they appear from this image. It is therefore not possible to estimate the total area of the open channels. To study these features more closely a focused-ion-beam (FIB) cross section has been prepared through several of these bubbles. Fig. 16 a) shows an overview image of the region where the cut was applied. Besides the bubbles, some "worm-like" remnants of the electro-polishing or grinding process are visible. They cause an uneven, wave-like tungsten surface, but apart from that, we assume that they are of no further consequence here. In Fig. 16 b), the cross section through the oxide film and some of the bubbles is shown. It becomes apparent that the oxide film is mostly intact and still has a thickness close to its original 100 nm. However, there are several holes or bubbles visible in the oxide film to the left and right side of the image. These bubbles, are located within the oxide film and do not reach into the underlying W bulk. However, for some of the bubbles, channels are visible that reach towards the surface. It seems likely that the bubbles are formed during D outgassing in one of two ways: a) outgassing of D forms clusters inside the oxide, which leads to D_2 filled cavity or b) the outgassing D reacts with the oxide film and creates heavy water (D_2O or HDO) filled cavities. In any case, the bubbles seem to eventually burst and create an open release channel towards the surface.

5. Summary

This present study aims to clarify which - if any - effect thin surface oxide films have on the D release from tungsten during thermal

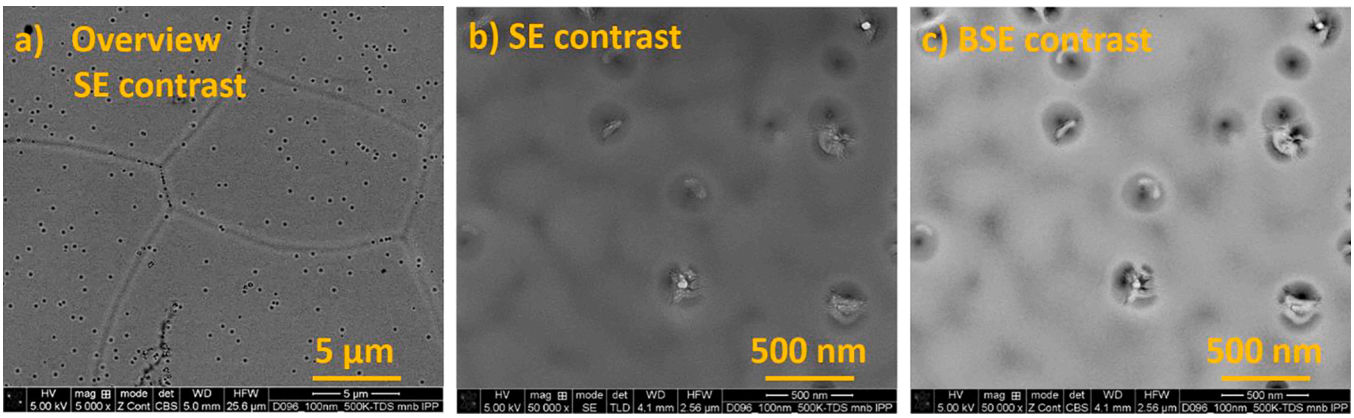

Fig. 15. SEM images of a 100 nm thick oxide film after the ramp-&-hold experiment to 500 K. In a) many small "hole-like" structures can been seen across the surface. They are more frequent along grain boundaries. In b) and c) enlarged views of these structures are shown in SE and BSE contrast, respectively. They appear to be burst bubbles, which are open towards the surface.

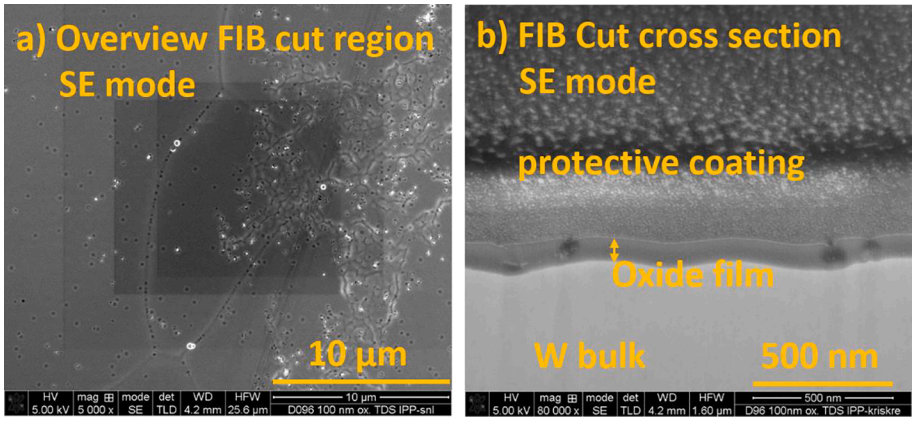

Fig. 16. SEM cross section image of the 100 nm thick sample after the ramp-&-hold experiment to 500 K. a) an overview image over the FIB cut region. Some artifacts of the electro-polishing are also present. b) Cross section image of the FIB cut. The "bubble-like" features in the oxide film are clearly visible and appear to have open channels towards the surface in some cases.

desorption spectroscopy (TDS) experiments. We addressed this question by a novel method that is based on a stable and well-quantifiable reservoir of deuterium in self-damaged tungsten underneath of electrochemically oxidized tungsten. Oxide film thicknesses ranged from 5 to 100 nm. The outgassing of D through the oxide film was analyzed with TDS up to 1000 K. The depth-resolved concentration profiles of D in the samples and the areal density of oxygen were measured with nuclear reaction analysis at all experimental steps. Changes of the morphology of the oxide film due to the outgassing of D were investigated with scanning electron microscopy (SEM).

We found that the thin oxide films significantly influence and alter the release behavior of D from W in several ways.

Already at about 475 K D starts to interact chemically with the oxide film and is released not only as HD or D_2 but also in the form of heavy water (HDO and D_2O). Above 700 K, this becomes the dominant release channel and D is released only in form of heavy water as long as enough oxide is available. This shows, that if oxide films are present, the heavy water signals (mass channels 19 and 20) have to be considered and quantified in order to obtain all information on the release energies of D from W. The effect of surface oxide films will be especially pronounced for experiments with low D retention. There even the natural oxide film (1–2 nm), that forms on W upon contact with air, may already influence the D release spectra.

SEM images show that the oxide film is strongly modified by the outgassing D and forms a complex two-dimensional structure. The thickest oxide films (50 and 100 nm) still cover the sample completely but show an inhomogeneous crystalline structure and some pinholes. Thinner films (25 nm), are partially removed and the remaining oxide forms snowflake-like structures on the metallic W. For 15 nm thick films, only small oxide islands remain on an otherwise metallic W surface and for even lower oxide thicknesses, the oxide is fully reduced and the metallic W surface is recovered. From the fact that at high temperatures D is only released as heavy water as long as oxygen remains on the surface, one can conclude that the mobility of D atoms at the surface is very high. Even D atoms that surface far (several µm) from an oxide island apparently travel along the surface to form an O-D group at the W oxide before they recombine with another D atom to be desorbed as water.

Furthermore, the oxide film influences the release spectra also at low temperature: the first D release peak at about 560 K (and especially its left flank that marks the beginning of strong D release) is shifted to higher temperature (or later times) with increasing oxide thickness. This indicates that the oxide film acts as a transport barrier for D release at temperatures above 475 K. At higher temperatures (above 650 K), the transport barrier effect is lost due to the (partial) reduction of the oxide.

This transport barrier effect has been further studied, by holding a sample with a 100 nm thick oxide film at 500 K during TDS. At this temperature, the chemical reaction between oxide and D sets in and the oxide film is reduced only slowly by the outgassing D. For a constant holding temperature of 500 K the oxide film acts as a bottleneck for the D release, as the total flux of outgassing D_2 is constant over the holding period and far smaller than for a reference sample with only natural

oxide. If the thermally triggered release of D from material defects would be the limiting factor for D outgassing from the sample, one would expect an exponential decay of the D signal at constant temperature. It is noteworthy however, that significant amounts of D (13% of the total initial content) are located within the oxide film itself after the hold experiment and D concentrations in the oxide film reach up to 4 %. This shows that the oxide film is not only a transport barrier but also a reservoir for D at 500 K. Furthermore, during the holding period (3.5 h), the slow reduction of the oxide leads to the formation of bubbles inside the oxide film. Eventually these bubbles burst open towards the surface and form channels through which molecular D can be released.

It is evident that oxide films have a strong effect on the release behavior of D from tungsten during TDS studies. From our results, we estimate that these effects become relevant for D release if the ratio of O atoms at the surface to D atoms in the sample is larger than 5–10 %. These results indicate that previous TDS studies on D release from W with higher ratios of O to D may have been influenced by (natural) surface oxide films. Thus, also the predications for D and Tritium retention/release in the plasma facing components (PFCs) of a future fusion reactor that are drawn from such studies may have been influenced in two ways. Firstly, the temperature of the D release peaks in TDS studies is relevant for calculating the binding energies of D in (neutron- or ion-induced) material defects in W. Any shift of these peaks due to the influence of surface oxide films represents a systematic error in the determination of these binding energies and thus leads to a distortion of the assumed HI retention and release values for hydrogen isotopes in the PFCs. Secondly, surface oxide films can lead to a significant part of the total D release being in form of heavy water due to chemical reaction of outgassing D with the oxide. Since heavy water signals are commonly not quantified (and neglected) in TDS studies on HI release from W, the total D release (and thus also the D retention) in W may have been systematically underestimated in the past. This is especially true for studies with only low D content or for studies with repeated air exposure in between measurement steps. In this cases a careful re-examination of the experiment conditions is advisable. For future TDS studies the O/D ratio should be monitored and ideally kept low in order to make reliable predictions on hydrogen isotope retention and release from W for a future fusion reactor.

CRediT authorship contribution statement

K. Kremer: Investigation, Formal analysis, Writing – original draft, Writing – review & editing, Visualization, Supervision. **M. Brucker:** Investigation, Formal analysis, Writing – original draft, Writing – review & editing, Visualization. **W. Jacob:** Writing – review & editing, Supervision, Resources, Funding acquisition. **T. Schwarz-Selinger:** Conceptualization, Methodology, Investigation, Formal analysis, Validation, Resources, Writing – original draft, Writing – review & editing, Supervision.

Declaration of Competing Interest

The authors declare that they have no known competing financial interests or personal relationships that could have appeared to influence the work reported in this paper.

Acknowledgement

We thank K. Hunger for her assistance in grinding and polishing the samples. We appreciate the assistance of M. Balden and S. Elgeti with operating the electron microscope. We further thank T. Dürbeck for his continuous support with the TDS setup and Klaus Schmid for providing the deconvolution program NRADC and his support in using it. We thank Joachim Dorner and Michael Fusseder for operating the accelerator for the tungsten irradiation and the ion beam analysis. Finally, we thank our division head Uli Stroth for his continuous interest and support of this study.

This work has been carried out within the framework of the EUROfusion Consortium and has received funding from the Euratom research and training programme 2014-2018 and 2019-2020 under grant agreement No 633053. The views and opinions expressed herein do not necessarily reflect those of the European Commission.

Appendix A. Supplementary data

Supplementary data to this article can be found online at https://doi.org/10.1016/j.nme.2022.101137.

References:

[1] G. De Temmerman, T. Hirai, R.A. Pitts, The influence of plasma-surface interaction on the performance of tungsten at the ITER divertor vertical targets, Plasma Phys. Controlled Fusion 60 (4) (2018) 044018, https://doi.org/10.1088/1361-6587/aaaf62.

[2] D. Stork, et al., Materials R&D for a timely DEMO: Key findings and recommendations of the EU Roadmap Materials Assessment Group, Fusion Eng. Des. 89 (7–8) (Oct. 2014) 1586–1594, https://doi.org/10.1016/j.fusengdes.2013.11.007.

[3] J. Roth, K. Schmid, Hydrogen in tungsten as plasma-facing material, Phys. Scr. T145 (2011) 014031, https://doi.org/10.1088/0031-8949/2011/T145/014031.

[4] T. Tanabe, Review of hydrogen retention in tungsten, Phys. Scr. T159 (2014) 014044, https://doi.org/10.1088/0031-8949/2014/T159/014044.

[5] W.R. Wampler, R.P. Doerner, The influence of displacement damage on deuterium retention in tungsten exposed to plasma, Nucl. Fusion 49 (11) (2009) 115023, https://doi.org/10.1088/0029-5515/49/11/115023.

[6] O.V. Ogorodnikova, V. Gann, Simulation of neutron-induced damage in tungsten by irradiation with energetic self-ions, J. Nucl. Mater. 460 (May 2015) 60–71, https://doi.org/10.1016/j.jnucmat.2015.02.004.

[7] M.J. Simmonds, T. Schwarz-Selinger, J.H. Yu, M.J. Baldwin, R.P. Doerner, G. R. Tynan, Isolating the detrapping of deuterium in heavy ion damaged tungsten via partial thermal desorption, J. Nucl. Mater. 522 (Aug. 2019) 158–167, https://doi.org/10.1016/j.jnucmat.2019.05.016.

[8] E.A. Hodille, F. Ghiorghiu, Y. Addab, A. Založnik, M. Minissale, Z. Piazza, C. Martin, T. Angot, L. Gallais, M.-F. Barthe, C.S. Becquart, S. Markelj, J. Mougenot, C. Grisolia, R. Bisson, Retention and release of hydrogen isotopes in tungsten plasma-facing components: the role of grain boundaries and the native oxide layer from a joint experiment-simulation integrated approach, Nucl. Fusion 57 (7) (2017) 076019, https://doi.org/10.1088/1741-4326/aa6d24.

[9] T. Schwarz-Selinger, J. Bauer, S. Elgeti, S. Markelj, Influence of the presence of deuterium on displacement damage in tungsten, Nuclear Materials and Energy 17 (Dec. 2018) 228–234, https://doi.org/10.1016/j.nme.2018.10.005.

[10] R. Bisson, S. Markelj, O. Mourey, F. Ghiorghiu, K. Achkasov, J.-M. Layet, P. Roubin, G. Cartry, C. Grisolia, T. Angot, Dynamic fuel retention in tokamak wall materials: An in situ laboratory study of deuterium release from polycrystalline tungsten at room temperature, J. Nucl. Mater. 467 (2015) 432–438, https://doi.org/10.1016/j.jnucmat.2015.07.028.

[11] S. Markelj, T. Schwarz-Selinger, A. Založnik, M. Kelemen, P. Vavpetič, P. Pelicon, E. Hodille, C. Grisolia, Deuterium retention in tungsten simultaneously damaged by high energy W ions and loaded by D atoms, Nuclear Materials and Energy 12 (2017) 169–174, https://doi.org/10.1016/j.nme.2016.11.010.

[12] B. Wielunska, M. Mayer, T. Schwarz-Selinger, A.E. Sand, W. Jacob, Deuterium retention in tungsten irradiated by different ions, Nucl. Fusion 60 (9) (2020) 096002, https://doi.org/10.1088/1741-4326/ab9a65.

[13] G.R. Longhurst, J. Ambrosek, Verification and Validation of the Tritium Transport Code TMAP7, Fusion Sci. Technol. 48 (1) (Aug. 2005) 468–471, https://doi.org/10.13182/FST05-A967.

[14] E.A. Hodille, et al., Macroscopic rate equation modeling of trapping/detrapping of hydrogen isotopes in tungsten materials, J. Nuclear Mater. 467 (1) (2014) 424–431, https://doi.org/10.1016/j.jnucmat.2015.06.041.

[15] K. Schmid, U. von Toussaint, T. Schwarz-Selinger, Transport of hydrogen in metals with occupancy dependent trap energies, J. Appl. Phys. 116 (13) (2014) 134901, https://doi.org/10.1063/1.4896580.

[16] M. Zibrov, S. Ryabtsev, Y.u. Gasparyan, A. Pisarev, Experimental determination of the deuterium binding energy with vacancies in tungsten, J. Nucl. Mater. 477 (Aug. 2016) 292–297, https://doi.org/10.1016/j.jnucmat.2016.04.052.

[17] M. Pečovnik, E.A. Hodille, T. Schwarz-Selinger, C. Grisolia, S. Markelj, New rate equation model to describe the stabilization of displacement damage by hydrogen atoms during ion irradiation in tungsten, Nucl. Fusion 60 (3) (2020) 036024, https://doi.org/10.1088/1741-4326/ab680f.

[18] A. Dunnand, M. Minissale, J. B. Faure, L. Gallais, T. Angot, and R. Bisson, *submitted to Nuclear Fusion*.

[19] C. Hopf, W. Jacob, V. Rohde, Oxygen glow discharge cleaning in nuclear fusion devices, J. Nucl. Mater. 374 (3) (Mar. 2008) 413–421, https://doi.org/10.1016/j.jnucmat.2007.10.001.

[20] V.K. Alimov, B. Tyburska, M. Balden, S. Lindig, J. Roth, K. Isobe, T. Yamanishi, Surface morphology and deuterium retention in tungsten oxide layers exposed to low-energy, high flux D plasma, J. Nucl. Mater. 409 (1) (2011) 27–32, https://doi.org/10.1016/j.jnucmat.2010.12.028.

[21] K. Kremer, T. Schwarz-Selinger, W. Jacob, Influence of thin tungsten oxide films on hydrogen isotope uptake and retention in tungsten – Evidence for permeation barrier effect, Nuclear Materials and Energy 27 (2021) 100991, https://doi.org/10.1016/j.nme.2021.100991.

[22] T. Schwarz-Selinger, Deuterium retention in MeV self-implanted tungsten: Influence of damaging dose rate, Nuclear Materials and Energy 12 (2017) 683–688, https://doi.org/10.1016/j.nme.2017.02.003.

[23] M. McCargo, J.A. Davies, F. Brown, RANGE OF Xe ^{133} AND Ar ^{41} IONS OF KEV ENERGIES IN TUNGSTEN, Can. J. Phys. 41 (8) (1963) 1231–1244, https://doi.org/10.1139/p63-120.

[24] *PLANSEE Metall GmbH – High Performance Materials, A-6600 Reutte, Austria. http://www.plansee.com.*

[25] A. Manhard, G. Matern, M. Balden, A Step-By-Step Analysis of the Polishing Process for Tungsten Specimens, PM 50 (1) (2013) 5–16, https://doi.org/10.3139/147.110215.

[26] S. Möller, D. Matveev, Y. Martynova, B. Unterberg, M. Rasinski, T. Wegener, A. Kreter, C.h. Linsmeier, Dynamic outgassing of deuterium, helium and nitrogen from plasma-facing materials under DEMO relevant conditions, Nucl. Fusion 57 (1) (2017) 016020, https://doi.org/10.1088/0029-5515/57/1/016020.

[27] A. Manhard, T. Schwarz-Selinger, W. Jacob, Quantification of the deuterium ion fluxes from a plasma source, Plasma Sources Sci. Technol. 20 (1) (2011) 015010, https://doi.org/10.1088/0963-0252/20/1/015010.

[28] A. Manhard, M. Balden, U. von Toussaint, Blister formation on rough and technical tungsten surfaces exposed to deuterium plasma, Nucl. Fusion 57 (12) (2017) 126012, https://doi.org/10.1088/1741-4326/aa82c8.

[29] S. Kapser, M. Balden, T.F. da Silva, S. Elgeti, A. Manhard, K. Schmid, T. Schwarz-Selinger, U. von Toussaint, Influence of sub-surface damage evolution on low-energy-plasma-driven deuterium permeation through tungsten, Nucl. Fusion 58 (5) (2018) 056027, https://doi.org/10.1088/1741-4326/aab571.

[30] K. Schlueter, M. Balden, Dependence of oxidation on the surface orientation of tungsten grains, Int. J. Refract Metal Hard Mater. 79 (Feb. 2019) 102–107, https://doi.org/10.1016/j.ijrmhm.2018.11.012.

[31] *Private communication with Janez Zavasnik and Vasyl Shvalya at Josef-Stefan-Institute, Jamova cesta 39, 1000 Ljubljana, Slovenia, 2021.*

[32] V. Nemanič, J. Zavašnik, V. Shvalya, M. Žumer, Hydrogen permeability of non-stoichiometric tungsten oxides, J. Nucl. Mater. 548 (2021) 152860, https://doi.org/10.1016/j.jnucmat.2021.152860.

[33] W. Jacob, T. Dürbeck, T. Schwarz-Selinger, U. von Toussaint, Bonding States of Hydrogen in Plasma-Deposited Hydrocarbon Films, C 6 (1) (Jan. 2020) 3, https://doi.org/10.3390/c6010003.

[34] E. Salançon, T. Dürbeck, T. Schwarz-Selinger, F. Genoese, W. Jacob, Redeposition of amorphous hydrogenated carbon films during thermal decomposition, J. Nucl. Mater. 376 (2) (May 2008) 160–168, https://doi.org/10.1016/j.jnucmat.2008.02.070.

[35] M. Brucker, K. Kremer, T. Schwarz-Selinger, W. Jacob, "To be published".

[36] M. Mayer, SIMNRA User's Guide, IPP Report 9/113, Max-Planck-Institut fuer Plasmaphysik, Garching, Germany, April 1997 http://hdl.handle.net/11858/00-001M-0000-0027-6157-F.

[37] M. Mayer, Improved physics in SIMNRA 7, Nucl. Instrum. Methods Phys. Res., Sect. B 332 (Aug. 2014) 176–180, https://doi.org/10.1016/j.nimb.2014.02.056.

[38] T.F. Silva, C.L. Rodrigues, M. Mayer, M.V. Moro, G.F. Trindade, F.R. Aguirre, N. Added, M.A. Rizzutto, M.H. Tabacniks, MultiSIMNRA: A computational tool for self-consistent ion beam analysis using SIMNRA, Nucl. Instrum. Methods Phys. Res., Sect. B 371 (2016) 86–89, https://doi.org/10.1016/j.nimb.2015.10.038.

[39] M. Guitart Corominas, T. Schwarz-Selinger, Experimental determination of the ^{16}O (^{3}He,p$_0$)^{18}F differential cross section, Nuclear Instruments and Methods in Physics Research Section B: Beam Interactions with Materials and Atoms 450 (Jul. 2019) 13–18, https://doi.org/10.1016/j.nimb.2018.05.018.

[40] M. Mayer, E. Gauthier, K. Sugiyama, U. von Toussaint, Quantitative depth profiling of deuterium up to very large depths, Nucl. Instrum. Methods Phys. Res., Sect. B 267 (3) (Feb. 2009) 506–512, https://doi.org/10.1016/j.nimb.2008.11.033.

[41] "Gestis Stoffdatenbank:http://gestis.itrust.de/nxt/gateway.dll/gestis_de/005920.xml?f=templates$fn=default.htm$3.0," Oct. 19, 2020.

[42] E. Lassner, W.-D. Schubert, Tungsten: Properties, Chemistry, Technology of the Element, Alloys, and Chemical Compounds, Springer US, Boston, MA, 1999, https://doi.org/10.1007/978-1-4615-4907-9.

[43] M. Mayer, RESOLNRA: A new program for optimizing the achievable depth resolution of ion beam analysis methods, Nucl. Instrum. Methods Phys. Res., Sect. B 266 (8) (Apr. 2008) 1852–1857, https://doi.org/10.1016/j.nimb.2007.11.071.

[44] *J.F. Ziegler, www.srim.org.*

[45] K. Schmid, U. von Toussaint, Statistically sound evaluation of trace element depth profiles by ion beam analysis, Nuclear Instruments and Methods in Physics Research Section B: Beam Interactions with Materials and Atoms 281 (Jun. 2012) 64–71, https://doi.org/10.1016/j.nimb.2012.03.024.

[46] F. Besenbacher, W. Möller, A note on the 3He+D nuclear-reaction cross section, Nucl. Instrum. Methods 168 (1980) 111–114.

[47] B. Wielunska, M. Mayer, T. Schwarz-Selinger, U. von Toussaint, J. Bauer, Cross section data for the D(3 He, p) 4 He nuclear reaction from 0.25 to 6 MeV, Nucl. Instrum. Methods Phys. Res., Sect. B 371 (Mar. 2016) 41–45, https://doi.org/10.1016/j.nimb.2015.09.049.

[48] E. Ozkan, S.-H. Lee, C.E. Tracy, J.R. Pitts, S.K. Deb, Comparison of electrochromic amorphous and crystalline tungsten oxide films, Sol. Energy Mater. Sol. Cells 79 (4) (Sep. 2003) 439–448, https://doi.org/10.1016/S0927-0248(03)00019-9.

[49] M. Zibrov, M. Balden, M. Dickmann, A. Dubinko, W. Egger, M. Mayer, D. Terentyev, M. Wirtz, Deuterium trapping by deformation-induced defects in tungsten, Nucl. Fusion 59 (10) (2019) 106056, https://doi.org/10.1088/1741-4326/ab3c7e.

[50] Y. Addab, C. Martin, C. Pardanaud, J. Khayadjian, K. Achkasov, D. Kogut, G. Cartry, G. Giacometti, M. Cabié, J.L. Gardarein, P. Roubin, Formation of thin tungsten oxide layers: characterization and exposure to deuterium, Phys. Scr. T167 (2016) 014036, https://doi.org/10.1088/0031-8949/T167/1/014036.

[51] J.A. Basford, Analysis of offgassed water: Calibration and techniques, Journal of Vacuum Science & Technology A: Vacuum, Surfaces, and Films 12 (4) (Jul. 1994) 1778–1781, https://doi.org/10.1116/1.579005.